Supporting Information

Understanding the Dual-Phase Synergy Mechanism in Mn_2O_3-Mn_3O_4 Catalyst for Efficient Li-CO_2 Batteries

Limin Liu[†], Libo Zhang[§], Ke Wang[†], Hu Wu[†], Heng Mao[†], Long Li[†], Zongjie Sun[†], Shiyao Lu[†], Dongyang Zhang[†], Wei Yu[†], Shujiang Ding[†‡]*

[†] Xi'an Key Laboratory of Sustainable Energy Materials Chemistry, Department of Applied Chemistry, School of Chemistry, Xi'an Jiaotong University, Xi'an 710049, China

[‡] Xi'an Jiaotong University & Shaanxi Quantong Joint Research Institute of New Energy Vehicles Power, Xi'an Jiaotong University, Xi'an 710049, China

[§] State of Laboratory of Electrical Insulation and Power Equipment, School of Electrical Engineering, Xi'an Jiaotong University, Xi'an 710049, China

Corresponding Author

* E-mail: dingsj@mail.xjtu.edu.cn

L. L., L. Z., and K. W. contributed equally to this work.

Thermogravimetric analysis (TGA) was performed to confirm the degree of Mn-BTC conversion at a heating rate of 10 °C per minute under an air environment. As shown in **Figure S1**, the first step of weight loss starts from room temperature to 200°C. The corresponding weight loss might be attributed to the removal of physisorbed moistures and solvent molecules. The 48.3% weight loss around 450°C is referred to the decomposition of Mn-BTC, and the residues (30.9%) were thermally stable Mn_2O_3.

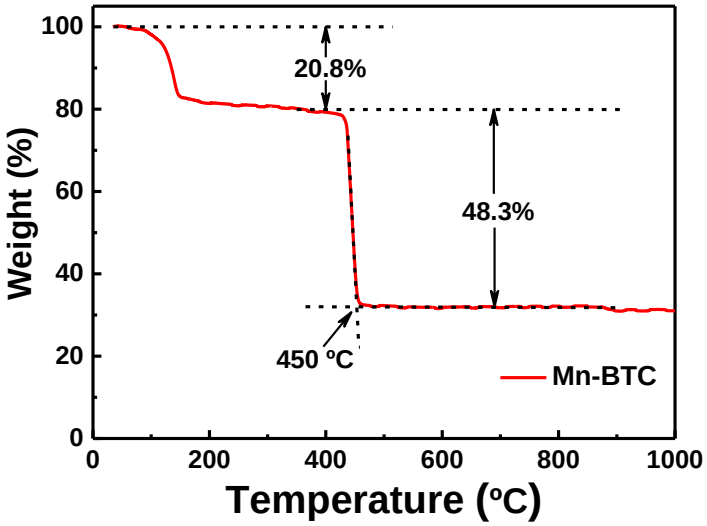

Figure S1. TGA curve of the Mn-BTC at a temperature ramp of 10 °C min^{-1}

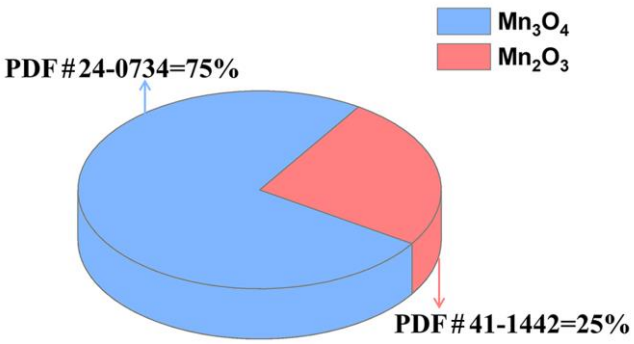

Figure S2. The content of Mn_2O_3 and Mn_3O_4 in the composite obtained by semi-quantitative analysis of XRD result.

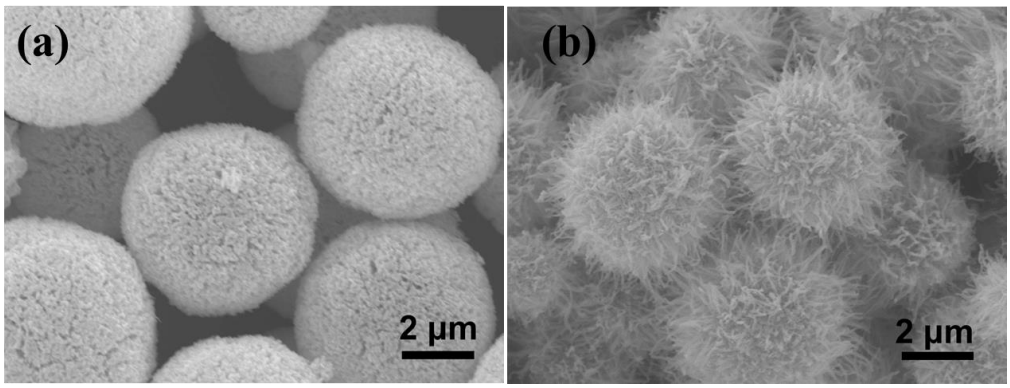

Figure S3. SEM images of (a) Mn-BTC and (b) Mn_2O_3.

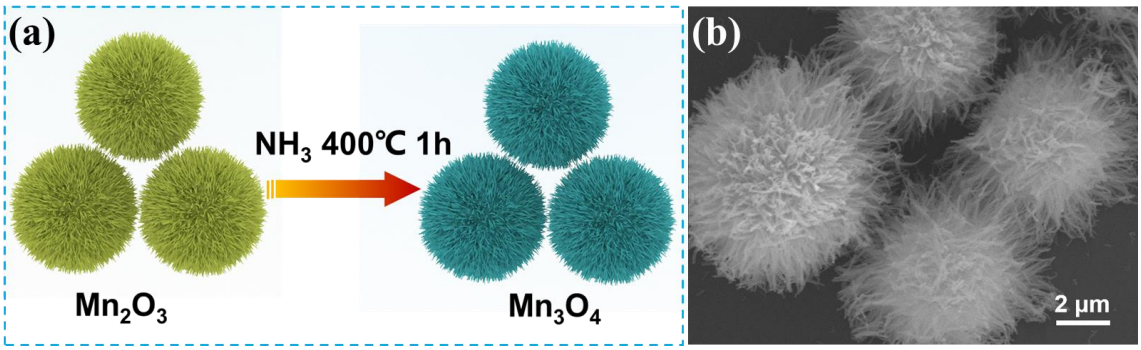

Figure S4. (a) Schematic illustration of the preparation of Mn_3O_4; (b) SEM image of Mn_3O_4.

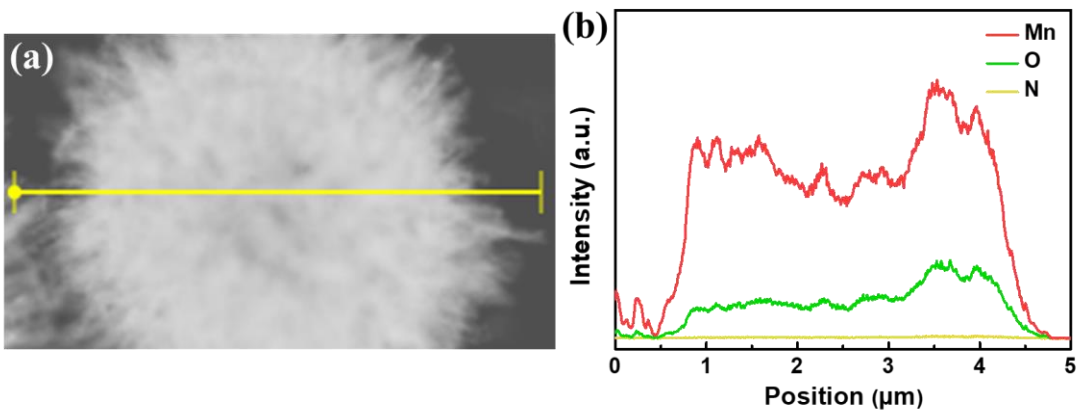

Figure S5. Mn_2O_3-Mn_3O_4: (b)line-scanning profiles of Mn, O, and N along with the red, green, and yellow line in (a), respectively.

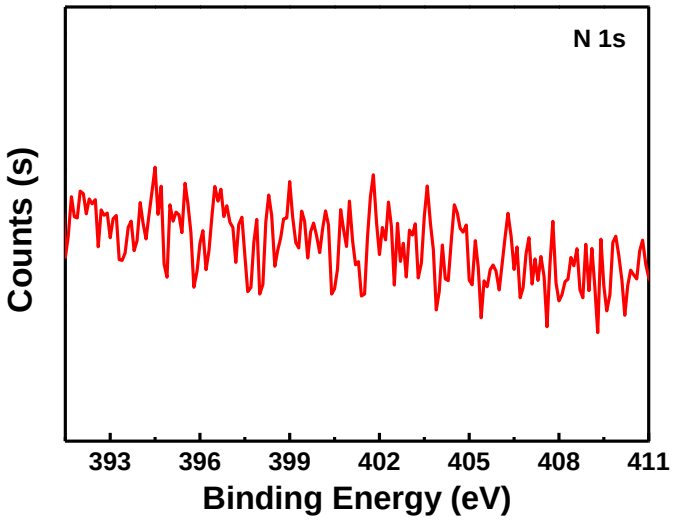

Figure S6. Refined N 1s XPS spectrum of Mn_2O_3-Mn_3O_4.

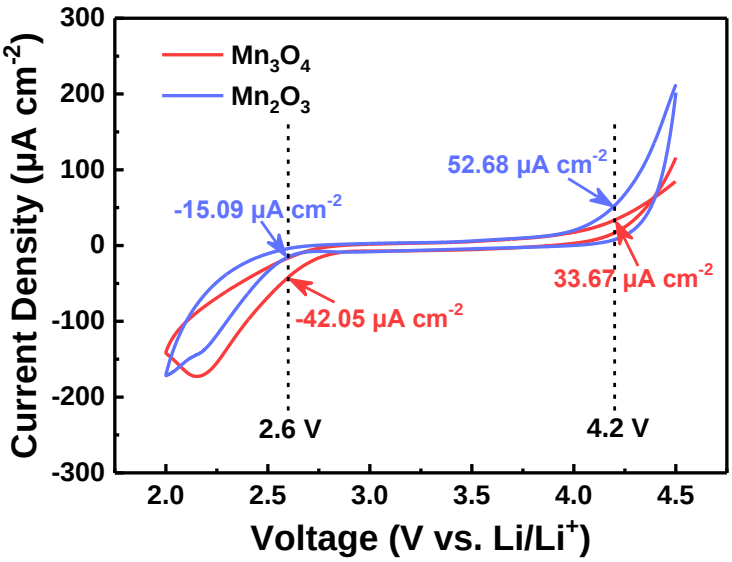

Figure S7. Cyclic voltammetry (CV) curves of Li-CO_2 batteries with Mn_2O_3 and Mn_3O_4 cathodes.

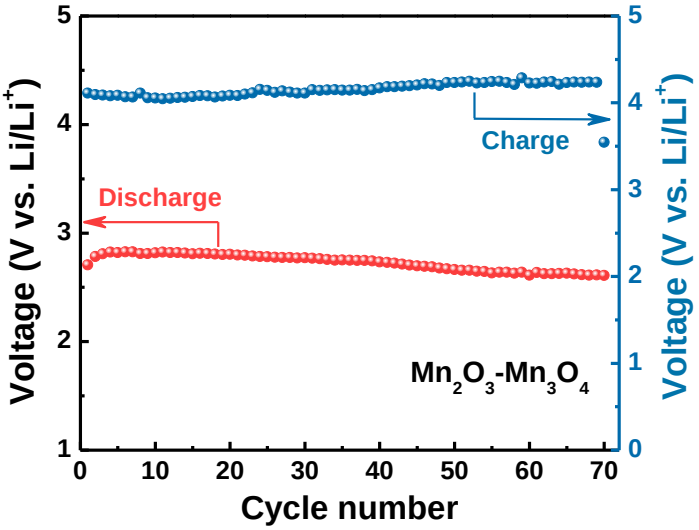

Figure S8. The median voltage of Li-CO_2 battery based on Mn_2O_3-Mn_3O_4 cathode during cycling at the current density of 100 mA g^{-1} within a limited capacity of 1000 mAh g^{-1}.

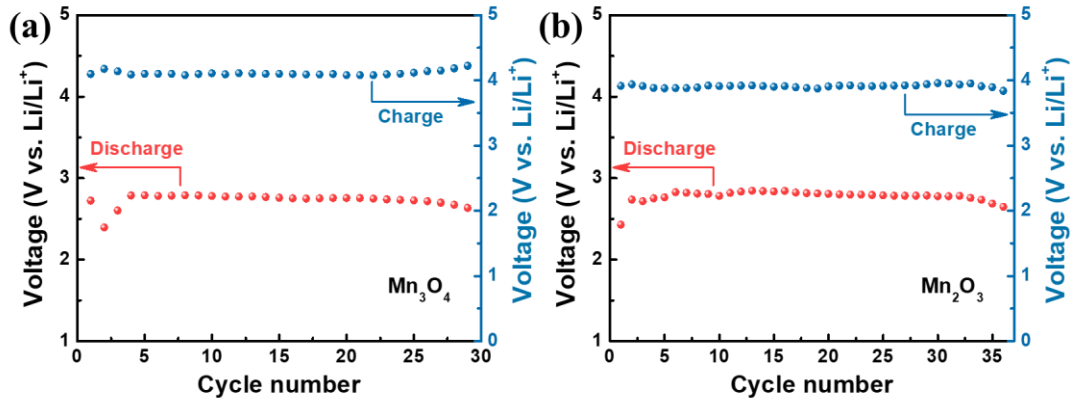

Figure S9. The median voltage of Li-CO_2 battery based on (a) Mn_2O_3 and (b) Mn_3O_4 cathode during cycling at the current density of 100 mA g^{-1} within a limited capacity of 1000 mAh g^{-1}.

Table S1. The comparisons of electrochemical performances between previous transition metal/carbon-based cathode catalysts

Cathode	Current density (mA g^{-1})	Discharge Capacity (mAh g^{-1})	Overpote-ntial (V)	Cycling number/ cycling time(hours)	Ref.
Mn_2O_3-Mn_3O_4	100	19024	~1.24	69/1380h	This work
Mn_2O_3	100	8261	~1.13	36/720h	This work
Mn_3O_4	100	14281	~1.33	29/580h	This work
Carbon nanotubes (CNTs)	50	8379	~1.6	29/1160h	1
Graphene	50	14722	~1.5	20/800h	2
Ketjen Black (KB)	30	1032	~1.6	7/467h	3
B,N-codoped holey graphene	1000	16033 (0.3 A g^{-1})	~1.75	200/436h	4
NiO / CNTs	50	9000	~1.55	42/1680h	5
Ni nanoparticles /N-doped graphene	100	17625	~1.75	100/2000h	6
Cu nanoparticles / N-doped graphene	200	14864	~1.4	50/500h	7
TiO_2@CNTs/CNF	0.05[a]	1.95[b]	~1.4	20/200h	8
NiFe@NC/PPC	0.05 [a]	6.8[b]	-	109/1090h	9
Mn_2(dobdc)	50	18022	~1.46	50/500h (200 mA g^{-1})	10
$Mn(HCOO)_2$	50	15510	~1.50	50/500h (200 mA g^{-1})	10
a-MnO_2 /CNTs	50	7134	-	50/1000h (100 mAg^{-1})	11
P-Mn_2O_3	50	9434	~1.40	50/2000h	12

[a] Unit: mA cm^2 [b] Unit: mA h cm^2

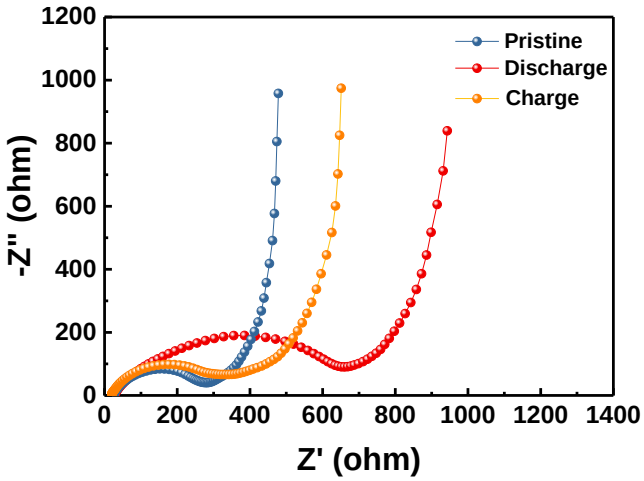

Figure S10. Nyquist plots of Li-CO_2 battery with Mn_2O_3-Mn_3O_4 cathode at different charge/discharge states.

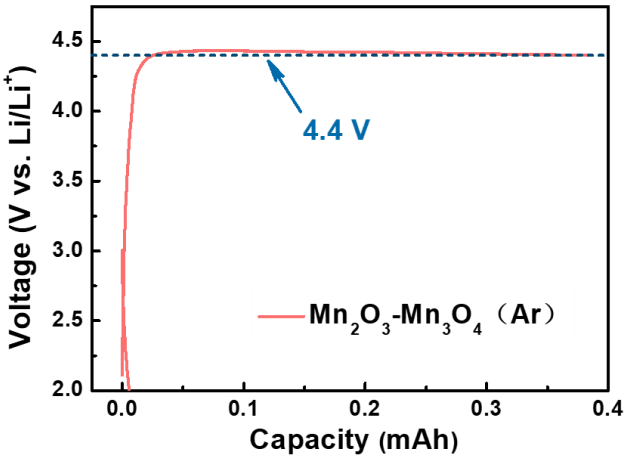

Figure S11. Discharge-charge curves of Li-CO_2 battery with Mn_2O_3-Mn_3O_4 cathode under Ar atmosphere at 100 mA g^{-1} over the voltage window of 2.0-4.5 V.

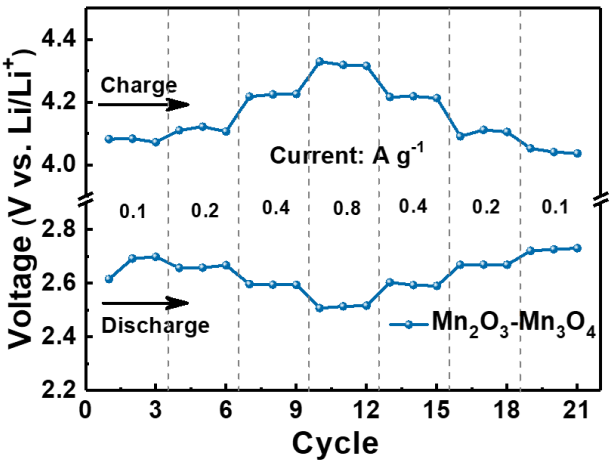

Figure S12. The rate capabilities of Li-CO_2 battery with Mn_2O_3-Mn_3O_4 cathode at different current densities.

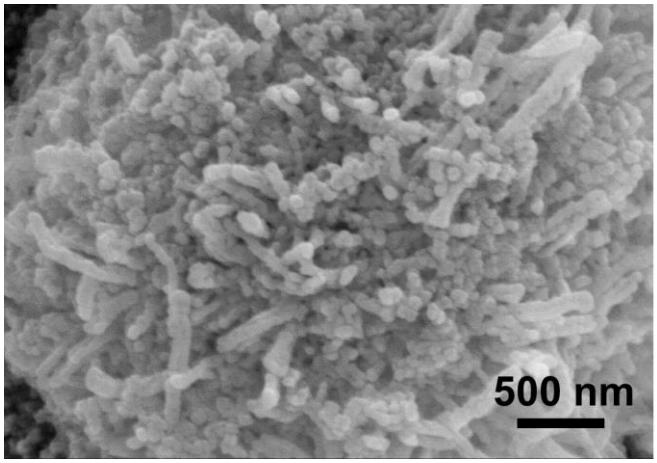

Figure S13. SEM image of Mn_2O_3-Mn_3O_4 cathode before cycles.

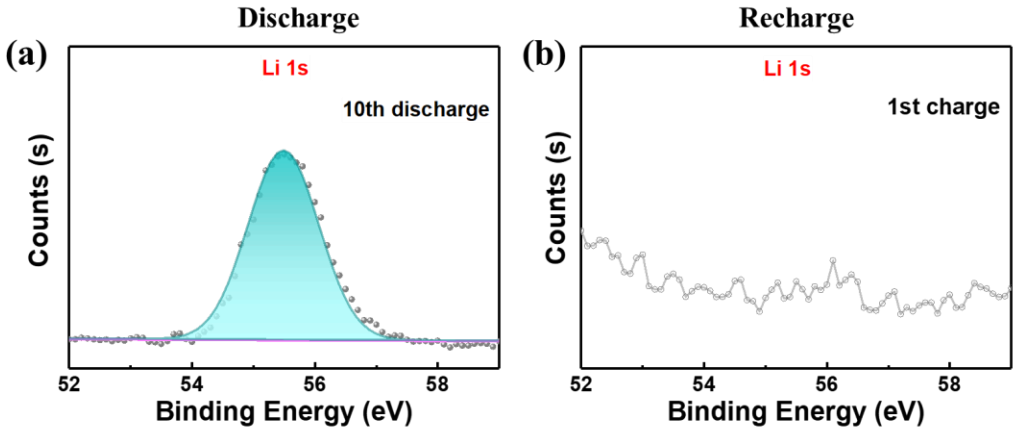

Figure S14. The high-resolution XPS spectra of Li 1s of the 10th cycle: (a) discharge and (b) recharge.

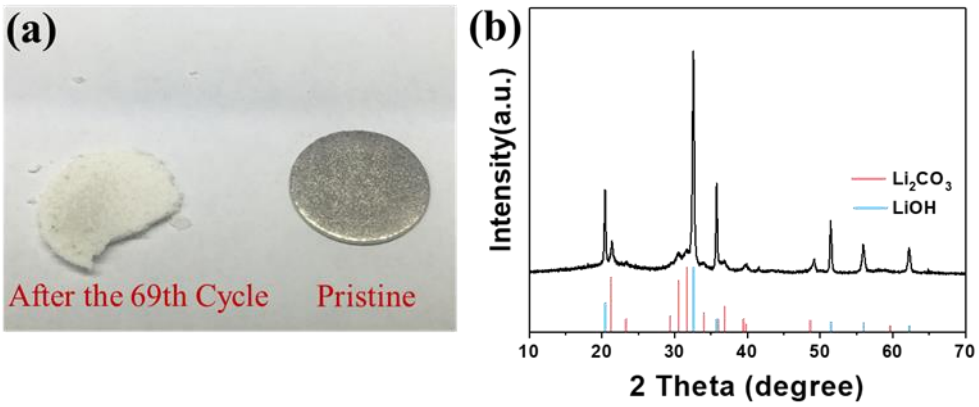

Figure S15. (a) Photographs of a pristine Li plate and a Li anode after the 69th cycle; (b) XRD spectra of Li anode after the 69th cycle.

The crystal faces of the surface models were chosen from our XRD and TEM results. XRD pattern (**Figure 2a**) reveals that the highest peak for Mn_2O_3 and Mn_3O_4 are (222) and (211), respectively. The TEM image indicates the exposure of (222) face for Mn_2O_3 and (101) face for Mn_3O_4. Therefore, these crystal planes were considered in this work.

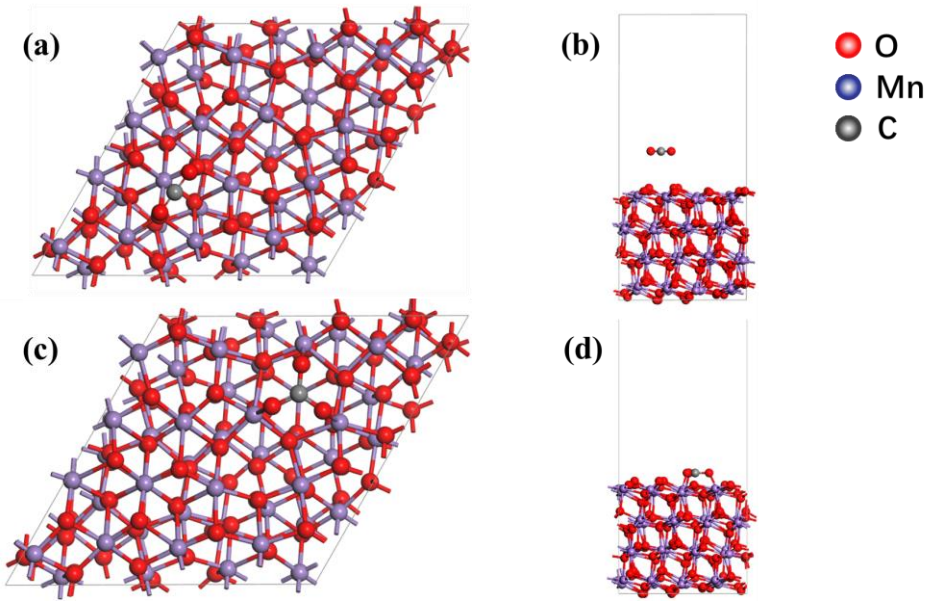

Figure S16. Side and top view of the optimized energetically most favorable structures of (a, b) CO_2 and (c, d) CO_3* adsorbed on Mn_2O_3 (222) surface.

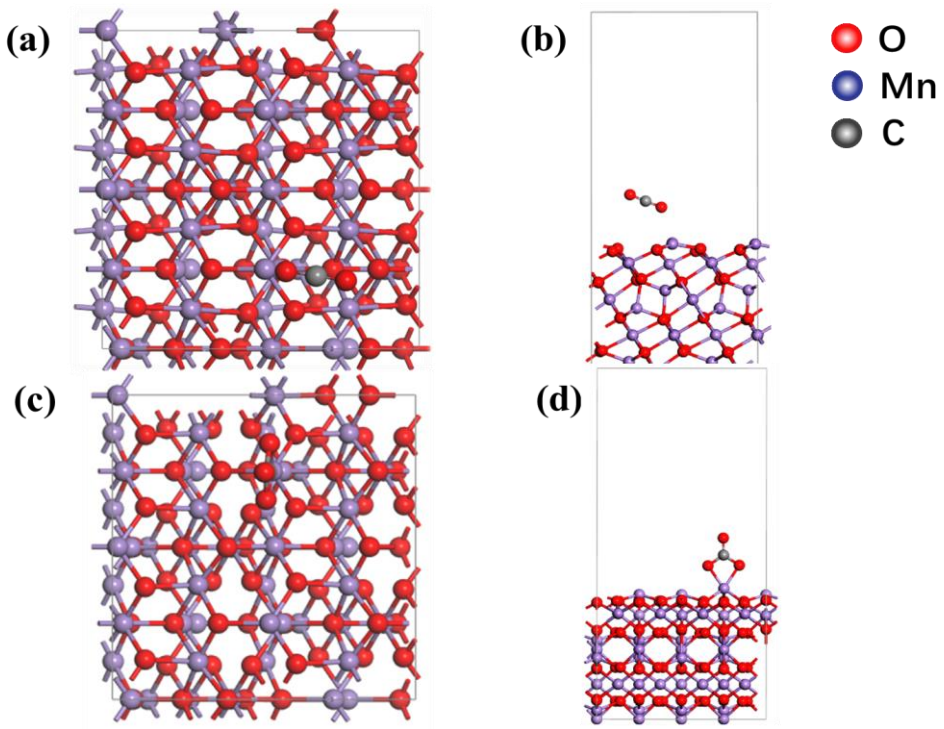

Figure S17. Side and top view of the optimized energetically most favorable structures of (a, b) CO_2 and (c, d) CO_3* adsorbed on Mn_3O_4 (101) surface.

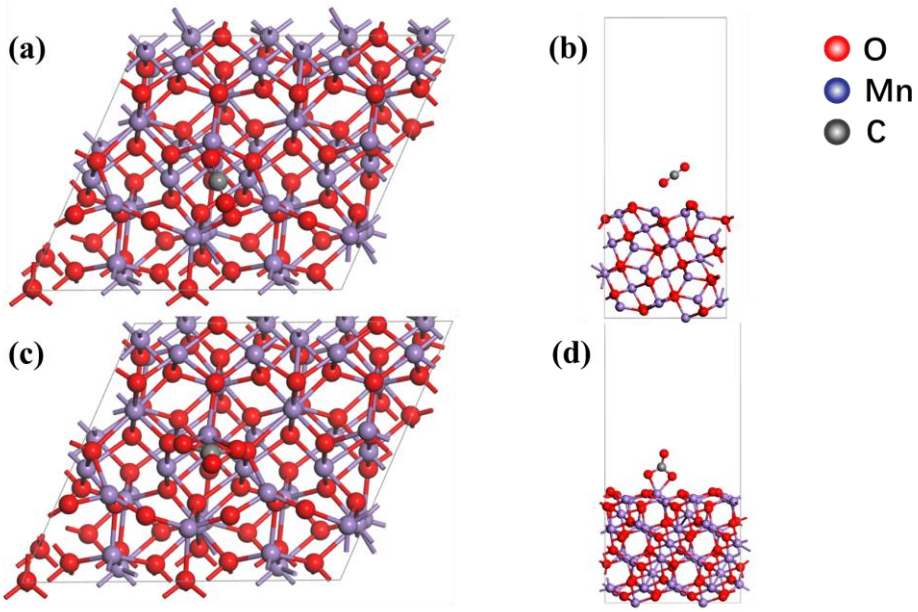

Figure S18. Side and top view of the optimized energetically most favorable structures of (a, b) CO_2 and (c, d) CO_3* adsorbed on Mn_3O_4 (211) surface.

References

(1) Zhang, X.; Zhang, Q.; Zhang, Z.; Chen, Y.; Xie, Z.; Wei, J.; Zhou, Z. Rechargeable Li-CO_2 batteries with carbon nanotubes as air cathodes. *Chem. commun.* **2015,** *51*, 14636-9.

(2) Zhang, Z.; Zhang, Q.; Chen, Y.; Bao, J.; Zhou, X.; Xie, Z.; Wei, J.; Zhou, Z. The First Introduction of Graphene to Rechargeable Li-CO_2 Batteries. *Angew. Chem., Int. Ed.* **2015,** *54*, 6550-6553.

(3) Liu, Y.; Wang, R.; Lyu, Y.; Li, H.; Chen, L. Rechargeable Li/CO_2–O_2 (2 : 1) battery and Li/CO_2 battery. *Energy Environ. Sci.* **2014,** *7*, 677.

(4) Qie, L.; Lin,Y.; J. Connell, W.; Xu, J.; Dai, L. Highly RechargeableLithium-CO_2 Batteries with aBoron- and Nitrogen-Codoped Holey-Graphene Cathode. *Angew. Chem., Int. Ed.* 2017 *56* 6970-6974.

(5) Zhang, X.; Wang, C.; Li, H.; Wang, X.-G.; Chen, Y.-N.; Xie, Z.; Zhou, Z. High performance Li–CO_2 batteries with NiO–CNT cathodes. *J. Mater. Chem. A* **2018,** *6*, 2792-2796.

(6) Zhang, Z.; Wang, X. G.; Zhang, X.; Xie, Z.; Chen, Y. N.; Ma, L.; Peng, Z.; Zhou, Z. Verifying the Rechargeability of Li-CO_2 Batteries on Working Cathodes of Ni Nanoparticles Highly Dispersed on N-Doped Graphene. *Advanced science* **2018,** *5*, 1700567.

(7) Zhang, Z.; Zhang, Z.; Liu, P.; Xie, Y.; Cao, K.; Zhou, Z. Identification of cathode stability in Li–CO_2 batteries with Cu nanoparticles highly dispersed on N-doped graphene. *J. Mater. Chem. A* **2018,** *6*, 3218-3223.

(8) Pipes, R.; Bhargav, A.; Manthiram, A. Nanostructured Anatase Titania as a Cathode Catalyst for Li-CO_2 Batteries. *ACS Appl. Mater. Interfaces* **2018,** *10*, 37119-37124.

(9) Liang, H.; Zhang, Y.; Chen, F.; Jing, S.; Yin, S.; Tsiakaras, P. A novel NiFe@NC-functionalized N-doped carbon microtubule network derived from biomass as a highly efficient 3D free-standing cathode for Li-CO_2 batteries. *Appl. Catal. B- Environ.* **2019,** *244*, 559-567.

(10) Li, S.; Dong, Y.; Zhou, J.; Liu, Y.; Wang, J.; Gao, X.; Han, Y.; Qi, P.; Wang, B. Carbon dioxide in the cage: manganese metal–organic frameworks for high performance CO_2 electrodes in Li–CO_2 batteries. *Energy Environ. Sci.* **2018,** *11*, 1318-1325.

(11) Lei, D.; Ma, S.; Lu, Y.; Liu, Q.; Li, Z. High-Performance Li-CO_2 Batteries with α-MnO_2/CNT Cathodes. *J. Electron. Mater*. **2019,** *48*, 4653-4659.

(12) Ma, W.; Lu, S.; Lei, X.; Liu, X.; Ding, Y. Porous Mn_2O_3 cathode for highly durable Li–CO_2 batteries. *J. Mater. Chem. A* **2018,** *6*, 20829-20835.